Journal of Inorganic Biochemistry 216 (2021) 111330

Contents lists available at ScienceDirect

Journal of Inorganic Biochemistry

journal homepage: www.elsevier.com/locate/jinorgbio

The interaction of half-sandwich (η^5-Cp*)Rh(III) cation with histidine containing peptides and their ternary species with (N,N) bidentate ligands

Azza A. Hassoon [a,1], Attila Szorcsik [a], Ferenc Bogár [b,c], Ibolya Zita Papp [b], Lívia Fülöp [b], Zoltán Kele [b], Tamás Gajda [a,*]

[a] Department of Inorganic and Analytical Chemistry, University of Szeged, Dóm tér 7, H-6720 Szeged, Hungary
[b] Institute of Medical Chemistry, University of Szeged, Dóm tér 8, H-6720 Szeged, Hungary
[c] MTA-SZTE Biomimetic Systems Research Group, University of Szeged, Dóm tér 8, H-6720 Szeged, Hungary

ARTICLE INFO

Keywords:
Half-sandwich rhodium(III)
His-peptides
Ternary complexes
Thermodynamic stability
Solution structure
DFT caculation

ABSTRACT

Our goal was to explore the possible interactions of the potential metallodrug (η^5-Cp*)Rh(III) complexes with histidine containing biomolecules (peptides/proteins) in order to understand the most important thermodynamic factors influencing the biospeciation and biotransformation of (η^5-Cp*)Rh(III) complexes. To this end, here we report systematic solution thermodynamic and solution structural study on the interaction of (η^5-Cp*)Rh(III) cation with histidine containing peptides and their constituents ((*N*-methyl)imidazole, GGA-OH, GGH-OH, histidine-amide, HGG-OH, GHG-NH_2), based on extensive ^{1}H NMR, ESI-MS and potentiometric investigations. The comparative evaluation of our data indicated that (η^5-Cp*)Rh(III) cation is able to induce the deprotonation of amide nitrogen well below pH 7. Consequently, at physiological pH the peptides are coordinated to Rh(III) by tridentate manner, with the participation of amide nitrogen. At pH 7.4 the (η^5-Cp*)Rh(III) binding affinity of peptides follow the order GGA-OH < < GGH-OH < < histidine-amide < HGG-OH < GHG-NH_2, i.e. the observed binding strength essentially depends on the presence and position of histidine within the peptide sequence. We also performed computational study on the possible solution structures of complexes present at near physiological pH. At pH 7.4 all histidine containing peptides form ternary complexes with strongly coordinating (N,N) bidentate ligands (ethylenediamine or bipyridyl), in which the peptides are monodentately coordinated to Rh(III) through their imidazole N^1-nitrogens. In addition, the strongest chelators histidine-amide, HGG-OH and GHG-NH_2 are also able to displace these powerful bidentate ligands from the coordination sphere of Rh(III).

1. Introduction

Due to their unique chemical properties, a number of half-sandwich organometallic compounds of transition metal ions with low spin d^6 electron configuration (Ru(II), Os(II), Rh(III), Ir(III)) have promising activity in various diseases, e.g. possess significant anticancer activity, even against cancers that are not responsive to platinum drugs [1–5]. Following the work made in the Sadler and Dyson research groups, a number of further (arene)Ru(II)-based compounds have been identified as potential candidates for clinical development [1–7]. Although, considerably less experimental data have been published for the isoelectronic (arene)Rh(III) compounds, several (η^5-Cp*)Rh(III) complexes exhibit higher in vitro activity than the related Ru(II) complexes or even cisplatin, at least against selected cancer cell lines [8–17]. In addition, its optimal ligand exchange kinetics make (η^5-Cp*)Rh(III) cation suitable drug delivery system for cytotoxins that are too toxic to be delivered directly, or have poor pharmacokinetics, such as curcumin [18].

These Ru/Rh-based compounds can act using both DNA or enzymes as target, but their molecular mechanisms of action have not yet been fully elucidated [1–7,19]. On the other hand, even DNA targeting compounds may interact with peptides/proteins during drug-transport, e.g. may undergo ligand substitution reactions especially in the blood plasma, before they reach the target site. It is therefore of high interest to study reactions between potential metallodrugs and biomolecules in order to understand their biodistribution, biotransformation and pharmacokinetic properties.

Increasing number of structural (MS/NMR [20–25], crystallographic

* Corresponding author.
E-mail address: gajda@chem.u-szeged.hu (T. Gajda).
[1] Presently PhD student at University of Szeged. Home affiliation: Chemistry Department, Faculty of Science, Mansoura University, Mansoura, 35516, Egypt.

https://doi.org/10.1016/j.jinorgbio.2020.111330
Received 21 September 2020; Received in revised form 23 November 2020; Accepted 1 December 2020
Available online 8 December 2020
0162-0134/

[26–32]) studies are available on the protein binding of [(arene)M(*ab*)c] compounds (where M = Ru(II), Rh(III); ab and c stand for bidentate and monodentate ligands, respectively). Since, different proteins under different conditions (pH, incubation time, ionic strength etc.) were studied, the reported data show rather promiscuous binding of (arene) Ru(II)/Rh(III) cations. Mainly His, Met, Cys and/or Glu sidechains are involved, and the proteins may coordinate by mono-, bi- and even tridentate manner. The latter indicates extensive degradation of [(arene)M (*ab*)c] complexes, even the arene ring can be lost [26]. Recently, the interaction of several (arene)Ru(II)/Rh(III) complexes with human serum albumin (HSA) has been studied [33]. HSA binds to 24 ± 3 uncomplexed (Cp*)Rh(III) cations, among them 8 were assumed to be amide coordinated, i.e. chelated by $\{N_{im},N^-_{amide}\}$ donors, but direct evidence of this binding mode was not obtained.

In order to understand the protein binding of (arene)Ru(II)/Rh(III) cations in more details amino acid and peptide complexes were also investigated. The [(arene)Mc_3] (c = H_2O or Cl^-) species form the usual mononuclear bi- and tridentate complexes with amino acids [34–37], while cysteine and penicillamine may form dinuclear complexes, too [38]. However, the interaction of amino acids with [(arene)M(*ab*)c] complexes strongly depends on the nature the bidentate ab ligands. For example, the $[(\eta^6\text{-biphenyl})Ru(en)Cl]^+$ cation reacts slowly with amino acids, and the order of reactivity is Cys > Met > His [20]. In contrast, (η^5-Cp*)Rh(III) and (η^6-*p*-cymene)Ru(II) complexes of flavanol derivatives show clear reactivity preference for His [13,25] (and Met [25]) over Cys.

Peptides behave similarly to proteins, the putative amino acid residues involved in the coordination are His [39,40], Met [40] and Cys [41], if available, with additional binding to Asp/Glu [20,40], and interestingly, the nitrogen atoms of the backbone amides were also hypothesized [21,40]. Several crystal structures of (Cp*)Rh(III) and (η^6-C_6Me_6)Ru(II) peptide complexes have been reported which include coordinated amide nitrogen(s) [34,42]. Since half-sandwich cations have only facial coordination sites, the central deprotonated amide nitrogen in $\{NH_2,N^-,N^-\}$ coordinated complexes is severely distorted towards a pyramidal conformation [42]. The solution structural study on $[(\eta^6\text{-}p\text{-cymene})Ru(II)]^{2+}$ complexes of His-peptides revealed histamine-like binding mode (HAVAHHH-NH_2 [43]) or $\{3N_{im}\}$ coordination (Ac-HAHH-NH_2, Ac-HAHAH-NH_2 [44]) in the physiologically relevant pH range, but amide coordination was not observed. Interestingly, the aromatic side chain of tyrosine can also interact with (η^5-Cp*)Rh(III) cation in water at pH 5–6 [45].

Solution thermodynamic data on peptide complexes of (arene)Ru (II)/Rh(III) cations are extremely rare in the literature. An indicator-displacement assay for the sequence-selective detection of His/Met-containing peptides has been developed [46] based on the different binding affinity of (η^5-Cp*)Rh(III) cation to peptides with different sequences, but only relative and apparent binding constants were reported. Besides, only (arene)Ru(II)/Rh(III) complexes of peptido-hydroxamic acids have been studied from solution thermodynamic point of view [47].

Our goal was to explore the possible interactions of potential metallodrug (η^5-Cp*)Rh(III) complexes with biomolecules (peptides/proteins), in order to understand the thermodynamic factors influencing the binding of (arene)Ru(II)/Rh(III) cations to peptides/proteins in aqueous solutions, as well as to investigate the possibility of amide coordination assumed by earlier studies [21,33,40]. As the imidazole ring of histidine side-chains is one of the main binding sites for (arene)Ru(II)/Rh(III) cations in proteines, first we performed systematic solution thermodynamic, solution structural and computational study on the binary complexes of (η^5-Cp*)Rh(III) cation with histidine containing peptides and their constituents ((*N*-methyl)imidazole ($\mathbf{L^{1(m)}}$), GGA-OH ($\mathbf{L^2}$), GGH-OH ($\mathbf{L^3}$), histidine-amide ($\mathbf{L^4}$), HGG-OH ($\mathbf{L^5}$), and GHG-NH_2 ($\mathbf{L^6}$), see Scheme 1). The primary reason for the selection of ligands was to study the coordination ability of imidazole ring to (η^5-Cp*)Rh(III) in different donor environments. Having explored the binary (η^5-Cp*)Rh(III)-peptide complexes, we also studied some (η^5-Cp*)Rh(III)-A-B ternary systems (where A = $\mathbf{L^2}$, $\mathbf{L^3}$, $\mathbf{L^4}$, $\mathbf{L^5}$ or $\mathbf{L^6}$ and B = 2,2′-bipyridyl or ethylenediamine) in order to mimic the interaction of the (η^5-Cp*)Rh (III)-based potentially anticancer or drug delivery agents with proteins. Although, the solution speciation of (η^5-Cp*)Rh(III) and (η^6-*p*-cymene) Ru(II) complexes show some differences due to their different hydrolytic properties [47], we believe that our results give valuable hints concerning the interaction of the extensively studied potentially anticancer

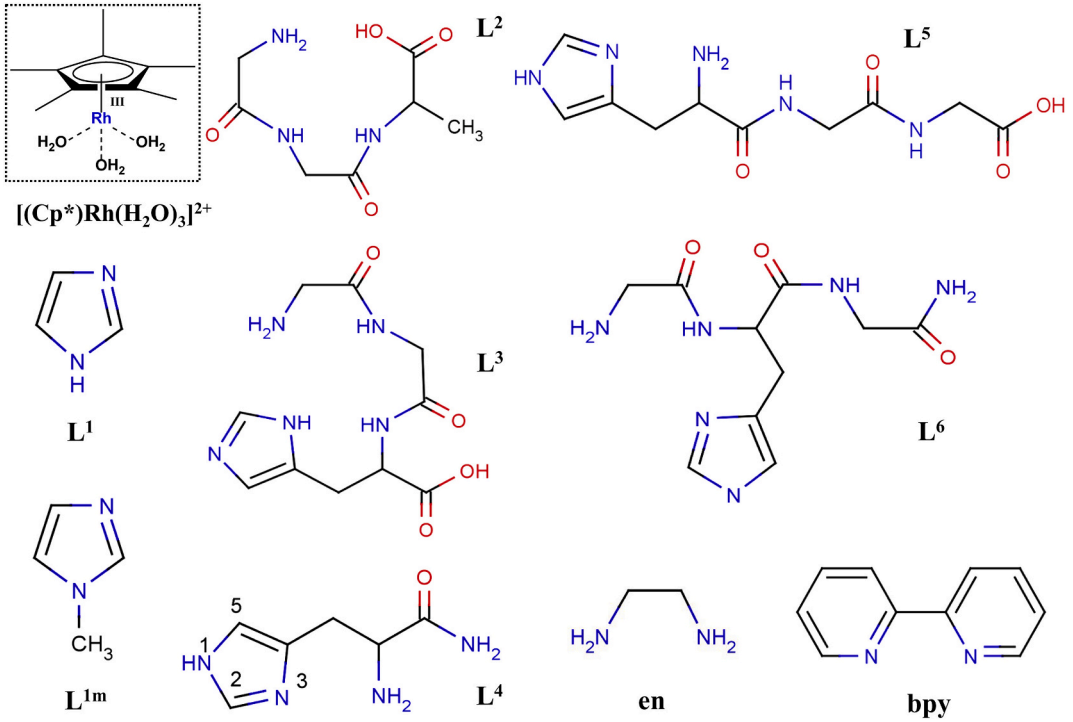

Scheme 1. Schematic structures of the studied ligands (the numbering of imidazole ring is shown for $\mathbf{L^4}$)

half-sandwich Ru(II) complexes with biomolecules, too.

2. Results and discussion

The p*K* values of the studied ligands (Table 1) agree very well with earlier reports [48]. In the following, the different systems are presented separately, the solution thermodynamic and solution structural properties of major complexes are discussed parallel, in the order of their appearance in solution with increasing pH.

2.1. Interaction of (η^5-Cp*)Rh(III) with imidazole (L^1) and N-methylimidazole (L^{1m})

The monodentate imidazol coordination is the most frequently detected binding mode of proteins to half-sandwich Ru(II)/Rh(III) complexes [23,26,29–33]. Indeed, (η^5-Cp*)Rh(III) forms rather stable $[ML^{1(m)}]^{2+}$, $[ML^{1(m)}{}_2]^{2+}$ and $[ML^{1(m)}{}_3]^{2+}$ complexes (here and in the following M stands for (η^5-Cp*)Rh(III) cation) up to the neutral pH range (Table 1, Fig. S1, see Supplementary Material). The formation constants of these parent complexes are nearly identical for the two ligands, and indicate somewhat lower stability than those of the related (η^6-p-cymene)Ru(II)-$\mathbf{L^{1m}}$ complexes [49]. Since Rh(III) is diamagnetic (low spin d^6 cation) in all our complexes, NMR is a straightforward method to gain information on the solution structure and also to support the solution speciation. Indeed, all $\mathbf{L^{1(m)}}$ complexes have slow exchange on the NMR timescale, and thus the changes in speciation can be easily followed (Fig. S2). Interestingly, in the (η^5-Cp*)Rh(III)-$\mathbf{L^1}$ system between pH 4–6 a broad signal appeared at 12 ppm (see the discussion on this signal below). Above pH 7–8 the two systems behave rather differently. In the (η^5-Cp*)Rh(III)-$\mathbf{L^{1m}}$ system the complex formation processes are fast enough for equilibrium study. In alkaline solution, a single additional species, $[MH_{-1}L^{1m}{}_2]^+$ (= $[M(OH)L^{1m}{}_2]^+$) could be detected. On the other hand, in the (η^5-Cp*)Rh(III)-$\mathbf{L^1}$ system the time needed to reach the equilibrium considerably increased above pH 7, which prevented the correct equilibrium study. After 24 h of equilibration at pH > 7 the ^{1}H NMR spectra indicate the formation of a great number of isomers (Fig. S2). Considering the difference between the two ligands, the most plausible reason of isomer formation is the metal-promoted deprotonation of the non-coordinated imidazole N^{1}H group of $\mathbf{L^1}$, and the subsequent formation of different oligomers via imidazolato bridges. The crystal structure of an imidazolato-bridged (η^5-Cp*)Rh(III) complex has been already reported in the literature [50].

2.2. Interaction of (η^5-Cp*)Rh(III) with GGA-OH (L^2)

In order to assess the effect of histidine moiety of tripeptides on (η^5-Cp*)Rh(III) binding, first we studied the complexes of GGA-OH peptide, having no coordinating side-chain. The combined potentiometric, UV–Vis and NMR results revealed the formation of four species between pH = 2–11 (Table 1, Fig. 1). The formation constants obtained reflect surprisingly high (η^5-Cp*)Rh(III) binding affinity of this simple peptide in the physiological pH range. The (η^5-Cp*)Rh(III) promoted deprotonation of N-terminal ammonium group takes places at four units lower pH than in the free ligand, confirming its strong binding to the metal ion. The important low field shift of ^{2}G-NH proton signal (8.55 → 9.22 ppm, see Fig. S3) in $[ML^2]^+$ suggests the formation of {NH_2,C=O,Cl^-} donor set, with the participation of ^{1}G amide oxygen. The next species ($[ML^2]^+$ = $[MH_{-1}L^2] + H^+$, pK = 5.80) is dominant in the solution between pH 7–9. Parallel with its formation the signal of ^{2}G amide disappeared from the spectrum (see Fig. S3), indicating its metal-promoted deprotonation, since the signal of ^{3}A amide is still present at pH 7.3. To our knowledge this is the first reported pK for amide nitrogen deprotonation of simple peptides promoted by a half-sandwich cation. The only related values, which have been determined for (η^5-Cp*)Rh(III) complexes of peptidohydroxamic acids [47], indicate similar pH range for (η^5-Cp*)Rh(III)-promoted amide deprotonation.

On the TOCSY (TOtal Correlation SpectroscopY) spectrum of $[MH_{-1}L^2]$ new peaks appeared around 4.45 ppm, which resulted strong cross-peaks with the ^{1}G-CH_2 proton signals (Fig. S4). Consequently, this new peaks belong to the terminal amino group, i.e. its proton-exchange with the solvent slows down considerably upon coordination. The

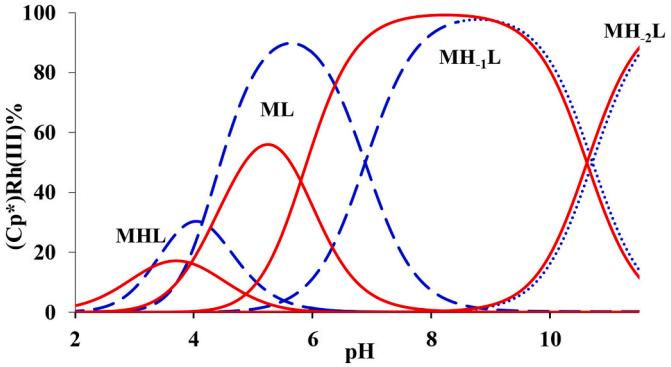

Fig. 1. Speciation in the (η^5-Cp*)Rh(III)-GGA-OH ($\mathbf{L^2}$, red lines) and (η^5-Cp*)Rh(III)-GGH-OH ($\mathbf{L^3}$, blue dashed lines) 1/1 systems (T = 298 K, I = 0.2 M KCl, [M]tot = 0.001 M). The curves of uncomplexed metal ion are not shown for clarity. In the case of GGH-OH the curve marked as 'MH$_{-1}$L' represents the sum of $[MH_{-1}L^3]$ and $[MH_{-1}L^3]_2$ complexes (see chapter 2.3.). Dotted lines show the region of slow processes, where only approximate speciation can be given. (For interpretation of the references to colour in this figure legend, the reader is referred to the web version of this article.)

Table 1
Protonation constants of the studied ligands, formation constants of their (η^5-Cp*)Rh(III) complexes and some derived data (T = 298 K, I = 0.20 M (KCl)), with estimated errors in parentheses (last digit). The constants in square brackets are only indicative values, since the systems were non-equilibrated.

	log β_{pqr}						
species (pqr)	$\mathbf{L^1}$	$\mathbf{L^{1m}}$	$\mathbf{L^2}$	$\mathbf{L^3}$	$\mathbf{L^4}$	$\mathbf{L^5}$	$\mathbf{L^6}$
H_3L (031)	–	–	–	17.45(2)	–	16.17(7)	–
H_2L (021)	–	–	11.25(2)	14.80(1)	12.90(1)	12.89(3)	14.50(2)
HL (011)	7.02(1)	7.10 (1)	7.98(1)	8.00(1)	7.48(1)	7.42(1)	8.23(1)
MHL (111)	–	–	10.63(8)	13.92(5)		14.88(1)	13.98(8)
ML (101)	5.83(2)	5.94(2)	6.68(3)	9.72(3)	11.09(5)	11.38(1)	–
ML_2 (102)	10.46(2)	10.68(2)	–	–	–	–	–
ML_3 (103)	13.43(3)	13.64(3)	–	–	–	–	–
$MH_{-1}L$ (1−11)	–	–	0.88(3)	2.75(4)	5.04(5)	5.89(11)	7.04(4)
$MH_{-2}L$ (1−21)	[−10.2]		−9.74(3)	[−8.1]	[−5.2]	[−4.6]	[−2.8]
$MH_{-1}L_2$ (1−12)	[2.6]	0.39(4)	–	–	–	–	–
$pK_{NH,\ amide}$	–	–	5.80	6.97	6.05	5.49	~ 3.5
$pM^*_{7.4}$	6.82	6.89	8.57	10.47	13.07	13.94	14.48

pM* values at pH 7.4 and at $c_M = c_L/10 = 1$ μM (T = 25 °C; I = 0.20 M (KCl), where $pM^* = -\log([M] + 2[M_2(OH)_2] + 2[M_2(OH)_3])$.

NOESY (Nuclear Overhauser Effect SpectroscopY) spectrum of $[MH_{-1}\mathbf{L^2}]$ revealed cross-peaks between the Cp*-CH_3 and ^{1}G-CH_2, ^{2}G-CH_2 protons, confirming the coordination of ^{1}G-amino and ^{2}G-amide nitrogens. On the other hand, the coordination of C-terminal carboxylate is not supported by our experimental data, i.e. the metal ion is coordinated by a $\{NH_2,N^-,Cl^-\}$ donor set.

Above pH 9 a further deprotonation was observed (pK = 10.62). During this process new set of peaks were not developed, only those of $[MH_{-1}\mathbf{L^2}]$ were shifted, indicating a fast-exchanging deprotonation. Although, the signal of ^{3}A amide proton disappeared from the spectra above pH 8, it is due to the acceleration of its proton exchange with the bulk water, since the coordination of this amide nitrogen would result in the development of a new set of peaks. The most obvious explanation of this process is the formation of mixed hydroxido complex, i.e. the $\{NH_2, N^-,OH^-\}$ coordinated $[MH_{-2}\mathbf{L^2}]^-$ species.

To assess the strength of (η^5-Cp*)Rh(III)-$\mathbf{L^2}$ interaction, it is worth examining the predominance diagram of the (η^5-Cp*)Rh(III)-Cu(II)-$\mathbf{L^2}$ ternary system (Fig. S5). In the physiological pH range the peptide is dominantly coordinated to (η^5-Cp*)Rh(III), i.e. its interaction with $\mathbf{L^2}$ is much stronger than that of the well-known peptide binder copper(II).

2.3. Interaction of (η^5-Cp*)Rh(III) with GGH-OH (L^3)

GGH-OH is an analogue of the N-terminal copper and nickel binding site of human serum albumin. Between pH 3–6 four distinct signals of Cp*-methyl protons can be detected on the ^{1}H NMR spectra (Fig. S6), two of which belong to $[MH\mathbf{L^3}]^{2+}$. This indicates the formation of isomers of this complex, either diastereomers or binding isomers. Surprisingly, two broad signals also appeared at 12.0 and 12.3 ppm on the ^{1}H NMR spectra (Fig. S6) up to pH 6 in 90% H_2O – 10% D_2O solution, which were absent in 100% D_2O. Similar signals were detected in the acidic pH-range for all imidazole derivatives, except for *N*-methylimidazole, and can be assigned to the N^{1}H proton of coordinated imidazole ring, whose proton exchange slowed down significantly due to the metal coordination of N^3-nitrogen. In the present case, the two signals belong to $[MH\mathbf{L^3}]^{2+}$ (12.0 ppm) and $[M\mathbf{L^3}]^+$ (12.3 ppm) complexes. Parallel with the formation of $[M\mathbf{L^3}]^+$ the signal of ^{2}G-NH is considerably shifted as compared to the free ligand (8.45 → 9.55 ppm, Fig. S6). The TOCSY spectrum observed at pH 5.6 indicates unusually high – approximately 400 Hz - inequivalence for the ^{1}G and ^{3}H methylene-protons (Fig. 2), which is likely due to the involvement of these methylene groups in rather rigid fused chelate ring(s). Remarkably, two peaks at 5.00 and 5.33 ppm are also appeared on the TOCSY spectrum resulting strong cross-peaks with the ^{1}G methylene-protons (Fig. 2), which therefore belong to the Rh(III) coordinated terminal amino group. Based on the NOESY spectrum, of the two imidazole CH protons, only C^{2}H is close to the Cp* methyl protons (Fig. S7). Besides, spatial proximity has been detected between Cp*-CH_3 and ^{3}H-C$_\beta$H$_2$, as well as between ^{3}H-C^{5}H and ^{1}G-NH_2 protons (Fig. S7). All these facts indicate tridentate $\{NH_2,C{=}O, N^3_{im}\}$ type coordination in $[M\mathbf{L^3}]^+$. Indeed, $[M\mathbf{L^3}]^+$ has considerably higher thermodynamic stability as compared to $[M\mathbf{L^2}]^+$ ($\log\beta_{101} = 6.68$ and 9.71 for $\mathbf{L^2}$ and $\mathbf{L^3}$, respectively), due to the additional imidazole coordination.

In turn, the enhanced stability of tridentate coordination in $M\mathbf{L^3}$ results in markedly higher pK for the next deprotonation ($[ML]^+ = [MH_{-1}L] + H^+$, $pK_{ML} = 5.80$ ($\mathbf{L^2}$) and 6.98 ($\mathbf{L^3}$), see Fig. 1). During this process the amide proton signal of ^{2}G disappeared from the ^{1}H NMR spectra (Fig. S6). Since the ^{3}H amide signals were still detectable, the Rh (III) promoted deprotonation of ^{2}G amide took place during this process. Interestingly, the deprotonation resulted in the duplication of signals, i.e. the formation of two isomers with nearly equal concentrations.

The EXSY (EXchange SpectroscopY) spectrum measured at pH 9.2 reflects that these isomers are in conformational or chemical exchange (Fig. 3A), i.e. are not diastereoisomers. The mass spectrum detected under identical conditions indicates the presence of a monomer and a dimer species in nearly equal amount (Fig. S8A), thus the exchange is related to the $2[MH_{-1}\mathbf{L^3}] = [MH_{-1}\mathbf{L^3}]_2$ equilibrium. The pH-metric titration curves can be well fitted by either the monomer or the dimer species, but the parallel refinement of β_{1-11} and β_{2-22} is not possible. However, assuming equal concentration of the monomer and dimer $\log\beta_{1-11} \sim 2.6$ and $\log\beta_{2-22} \sim 8.6$ can be estimated. Based on the NOESY spectrum, both CH protons of the imidazole ring (C^{2}H and C^{5}H) of both

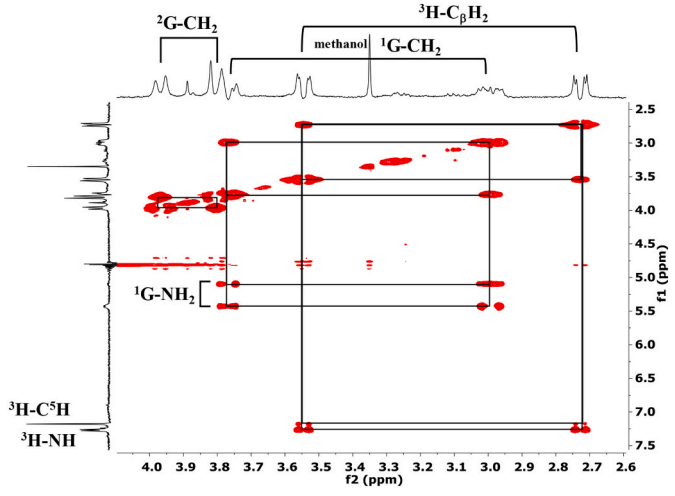

Fig. 2. Part of TOCSY spectrum of the (η^5-Cp*)Rh(III)-$\mathbf{L^3}$ 1:1 system at pH 5.67.

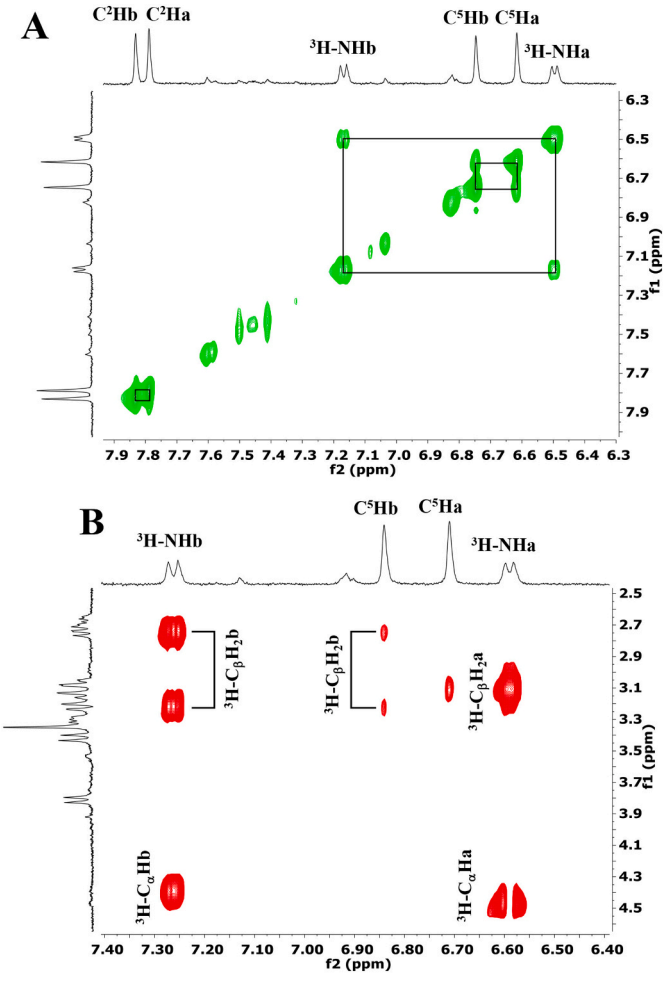

Fig. 3. Parts of EXSY (A) and TOCSY (B) spectra of the (η^5-Cp*)Rh(III)-$\mathbf{L^3}$ 1:1 system at pH 9.35.

complexes are in spatial proximity to the Cp* methyl protons (Fig. S8B). This is only possible if the N^1 nitrogen of imidazole ring is coordinated to Rh(III). In addition, the ^{1}G-CH_2 protons are also close to the Cp* methyl protons, suggesting {NH_2,N^-,N^1_{im}} type coordination in both species. In one of these complexes the histidine $C_\beta H_2$ protons are slightly, in the other they are considerably inequivalent (Fig. 3B). In the monomer complex the imidazole group is part of a 10-membered, rather strained macrochelate ring (Fig. 4A), and its reduced chelate effect allows the formation of dimer species. In $[MH_{-1}\mathbf{L^3}]_2$ the imidazole rings bind to the adjacent (η^5-Cp*)Rh(III), resulting in a more relaxed conformation of the histidine side chains (Fig. S18), thus the dimer has probably the more equivalent histidine $C_\beta H_2$ protons (signals marked by 'a' in Fig. 3).

Above pH 8 a further deprotonation was detected (pK ~ 11), but the complex formation processes become too slow for equilibrium study. At pH 11.6 at least nine peaks appeared in the region of Cp* methyl protons (Fig. S6), indicating the formation of several isomers, but structural details could not be extracted.

2.4. Interaction of (η^5-Cp*)Rh(III) with histidine-amide (L^4) and HGG-OH (L^5)

Both ligands are simple model of N-terminal histidine unit in proteins. In the (η^5-Cp*)Rh(III)-$\mathbf{L^4}$ system three complexes can be identified between pH 2–12 (Table 1, Fig. 5). The broad signal related to the N^1H proton of coordinated imidazole ring appeared on the ^{1}H NMR spectra between pH 2–6 in this case, too (Fig. 6A). The formation constant of $[M\mathbf{L^4}]^{2+}$ complex is much higher than the analogous values of $[M\mathbf{L^1}]^{2+}$, $[M\mathbf{L^2}]^{+}$ or $[M\mathbf{L^3}]^{+}$, indicating the coordination of both N^3_{im} and amino nitrogens within a 6-membered chelate. Since the resonances of amide protons did not change between pH 2–4, the coordination of carbonyl oxygen is unlikely. Therefore the metal ion in $[M\mathbf{L^4}]^{2+}$ has {NH_2,N^3_{im}, Cl^-} donor set, with bidentate, histamine-like coordination of $\mathbf{L^4}$.

Above pH 4 a new set of peaks developed on the ^{1}H NMR spectra (Fig. 6A), belonging to the $[MH_{-1}\mathbf{L^4}]^{+}$ species (pK = 6.05). As in the previous cases, new signals appeared on the ^{1}H NMR spectra close to the water resonance. In fact, the signal closest to water (at 4.90 ppm) is obscured and only its cross peaks appeared on the 2D spectra (Fig. 6B). The peaks at 4.90 and 5.15 ppm show spatial proximity to the C_α-H proton (Fig. S9A), thus belong to the coordinated amino-NH_2, while the resonance at 5.53 ppm is related to the deprotonated (and coordinated) amide-NH^-. The coordination of these nitrogens is further supported by the spatial proximity of their protons to the Cp*-methyl protons (Fig. S9). On the other hand, among the two imidazole CH protons, only C^2H shows vicinity to the Cp*-ring, which clearly indicates {N^3_{im},NH_2, NH^-} binding mode in $[MH_{-1}\mathbf{L^4}]^{+}$ (Fig. 4B).

The (η^5-Cp*)Rh(III)-$\mathbf{L^5}$ system behaves analogously. The formation

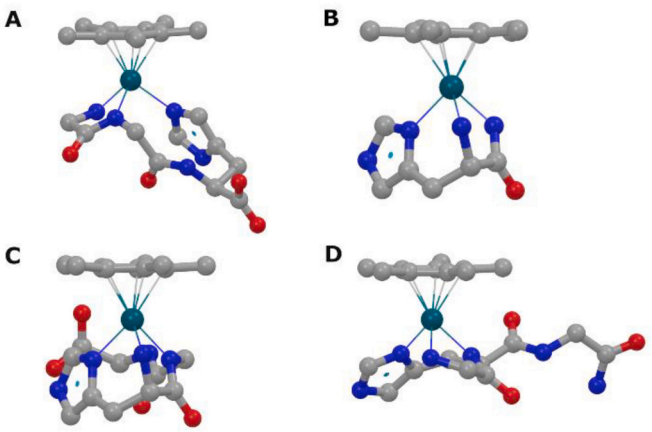

Fig. 4. Optimized structures of the $R_{Rh}S_{\alpha C}$ diastereomers of $MH_{-1}\mathbf{L^3}$ (A), $MH_{-1}\mathbf{L^4}$ (B), $MH_{-1}\mathbf{L^5}$ (C) and $MH_{-1}\mathbf{L^6}$ (D). See chapter 2.7.

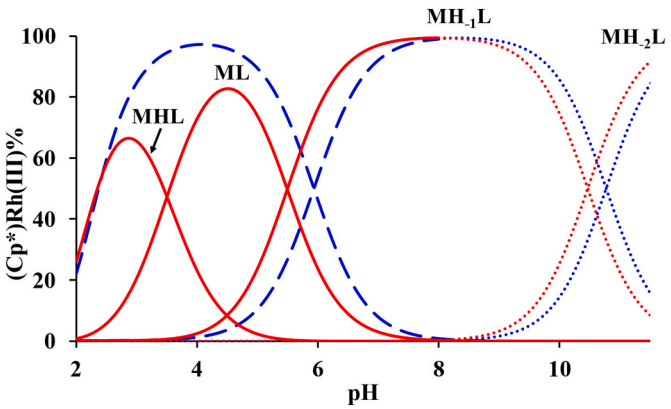

Fig. 5. Speciation in the (η^5-Cp*)Rh(III)-$\mathbf{L^4}$ (blue dashed lines) and (η^5-Cp*)Rh (III)-$\mathbf{L^5}$ (red lines) 1/1 systems (T = 298 K, I = 0.2 M KCl, $[M]_{tot}$ = 0.001 M). The curves of uncomplexed metal ion are not shown for clarity. Dotted lines indicate the region of slow processes, where only approximate speciation can be given. (For interpretation of the references to colour in this figure legend, the reader is referred to the web version of this article.)

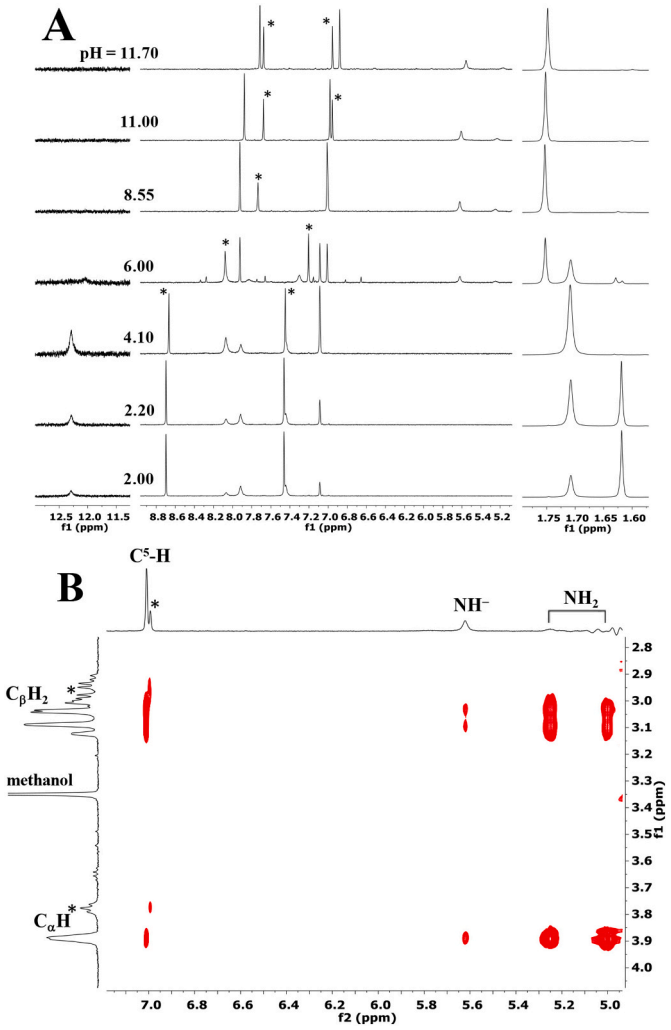

Fig. 6. Parts of pH-dependent ^{1}H NMR spectra (A) and TOCSY spectrum at pH 8.55 (B) of (η^5-Cp*)Rh(III)-$\mathbf{L^4}$ 2/3 system (asterix denotes the signals of the free ligand).

constants of $[ML^4]^{2+}$ and $[ML^5]^{+}$ complexes are very similar, and the imidazole N^1H proton appeared on the ^1H NMR spectra of both $[MHL^5]^{2+}$ and $[ML^5]^{+}$ (Fig. S10A), confirming the coordination of N^3 nitrogen in these species. The pK of $[MHL^5]^{2+}$ (pK = 3.50) is close to the pK of carboxylate in the free ligand (Table 1). Consequently, in both $[MHL^5]^{2+}$ and $[ML^5]^{+}$ the ligand binds to the metal ion with histamine-like $\{NH_2,N^3_{im}\}$ coordination, they differ only in the protonation state of the C-terminal carboxylate, remote from the metal ion.

During the deprotonation of $[ML^5]^{+}$ species (pK = 5.49) the signal of ^2G amide proton disappeared from the ^1H NMR spectrum. Like in the previous cases, parallel with this amide deprotonation new signals appear near the water, which show strong TOCSY cross-peaks with histidine C^5H, $C_\alpha H$ and $C_\beta H_2$ protons, and therefore belong to the coordinated N-terminal amino group (Fig. S10B). Among the two imidazole CH protons, only the C^2H proton exhibits spatial proximity to the Cp* methyl protons, thus the N^3 nitrogen of the imidazole ring is coordinated in $MH_{-1}L^5$. Besides, the ^1H-NH_2, ^2G-CH_2 and ^3G-NH protons are also close to the Cp* ring (Fig. S9B), confirming the Rh(III)-promoted deprotonation of ^2G amide, and therefore the $\{N^3_{im},NH_2,N^-\}$ binding mode in $MH_{-1}L^5$ (Fig. 4C).

Above pH 8 a further deprotonation was observed in both systems, leading to $MH_{-2}L$ in slow processes. During these deprotonations new set of peaks did not appear, only those already present were shifted (Figs. 6A and S10), i.e. this deprotonation does not alter the coordination sphere of Rh(III). Two of such processes may take place, the deprotonation of the amino or imidazole N^1-nitrogens. Since the imidazole C^2H and C^5H protons show the largest shift between pH 8–12, and the signals of coordinated amino group are less affected, this deprotonation is probably related (at least for the most part) to the imidazole N^1-nitrogen.

2.5. Interaction of (η^5-Cp*)Rh(III) with GHG-NH_2 (L^6)

In this peptide the histidine is in the second position, and since it was prepared in our laboratory, the C-terminal carboxylate is amidated. After the formation of a minor species $[MHL^6]^{3+}$ between pH 2–4, two strongly cooperative deprotonations have been detected. Consequently, the formation of $[ML^6]^{2+}$ could not be observed, only that of the subsequent $[MH_{-1}L^6]^{+}$ complex (Fig. S11), which is the only species in the solution between pH 4.5–8. Up to pH 4.43 the ^2H amide proton gradually disappeared, while the signals of terminal (^1G) NH_2 and imidazole N^1H protons appeared on the NMR spectra (Figs. 7 and S12). The NOESY spectrum indicates spatial proximity between the Cp*-methyl and imidazole C^2H, ^3G amide (Fig. 7B), ^1G-NH_2, ^1G-CH_2 as well as ^2H-$C_\beta H_2$ protons (Fig. S13). All these facts confirm the $\{NH_2,N^-,N^3_{im}\}$ type coordination of peptide in $[MH_{-1}L^6]^{+}$ species. This is somewhat surprising considering that L^6 in this binding mode prefers meridional, while (η^5-Cp*)Rh(III) prefers facial coordination. Therefore, we suspected dimer formation, similar to the case of GGH-OH (L^3). However, the MS spectrum at pH 5 clearly indicates the sole presence of the monomer $[MH_{-1}L^6]^{+}$ complex (Fig. S14). The crystal structures of tridentate $\{NH_2,N^-,N^-\}$ coordinated (Cp*)Rh(III)-peptide complexes indicate that the central deprotonated amide nitrogen is distorted towards a pyramidal conformation [42]. Probably, the high thermodynamic stability over-compensates this conformational strain. Indeed, the potentiometric data show outstanding stability of the amide-coordinated complex of L^6, its formation takes place at 3–4 units lower pH than in the former systems.

Interestingly, in the (η^5-Cp*)Rh(III)-L^6 system a minor diastereomer ($R_{Rh}S_{\alpha C}$ or $S_{Rh}S_{\alpha C}$) also appeared beside the major one. This resulted in the duplication of signals, which can be clearly seen e.g. on the imidazole CH and Cp*-methyl signals (see Fig. S12 and further discussion on the diastereomers in chapter 2.7.).

In this system, too, an additional deprotonation was observed above pH 8, which process was proved to be very slow, the equilibrium was not reached even after several days. In this case, however, the slow complex formation process was further complicated by the slow hydrolysis of the C-terminal amide group, which can be clearly seen on the time dependent MS spectrum at pH 11.04 (Fig. S15). This hydrolysis is obviously related to the coordinated metal ion, but the exact mechanism is unknown.

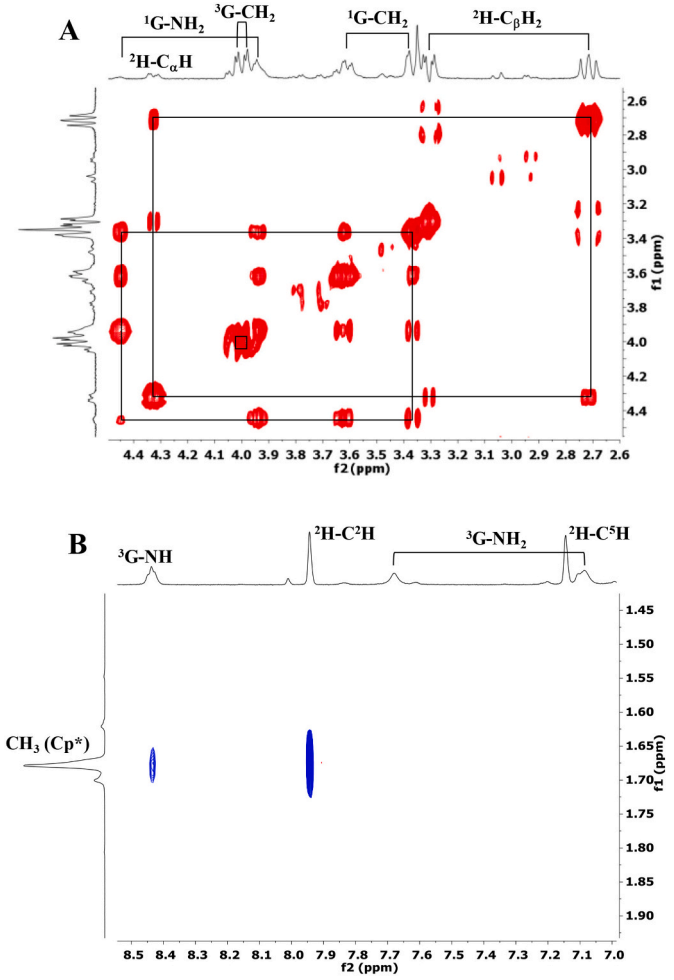

Fig. 7. Parts of TOCSY (A) and NOESY (B) spectra of the (η^5-Cp*)Rh(III)-L^6 1:1 system at pH 4.43.

2.6. Comparison of equilibrium data and competition with strongly coordinating bidentate ligands

Due to the different basicity of the ligands and composition of their complexes, it is more appropriate to calculate the concentration of non-peptide bound metal ion (pM* = $-\log([M] + 2[M_2(OH)_2] + 2[M_2(OH)_3])$ at pH 7.4 and at $10 \times [M]_{tot} = [L]_{tot} = 10^{-5}$ M, in order to compare the metal ion binding abilities of the studied ligands (Table 1). Obviously, the monodentate L^1 and L^{1m} have the lowest metal binding affinity, which are followed by GGA-OH (L^2). The coordination ability of histidine containing peptides strongly depends on the position of His unit. Such dependency has already been identified for copper(II) complexes (HGG < GHG ≤ GGH [51,52]), however the different structural preferences of the two metal ions resulted in different stability order in the present case. The ATCUN-related GGH (L^3) is the weakest (η^5-Cp*)Rh(III) binder (Table 1), since only three binding sites of Rh(III) half-sandwich cation are available, in a facial geometry. On the other hand, histidine-amide (L^4) and HGG (L^5) provide tridentate facial $\{NH_2, N_{im},N^-\}$ coordination, therefore these ligands have considerably higher (η^5-Cp*)Rh(III) binding affinity. Interestingly, GHG-NH_2 (L^6) is the strongest (η^5-Cp*)Rh(III) binder, despite its preference for meridional

geometry.

Having explored the binary (η^5-Cp*)Rh(III)-peptide complexes, we also studied some (η^5-Cp*)Rh(III)-A-B ternary systems (where A = **L²**, **L³**, **L⁴**, **L⁵** or **L⁶**; B = 2,2′-bipyridyl (bpy) or ethylene-diamine (en)), in order to mimic the interaction of the (η^5-Cp*)Rh(III)-based potentially anticancer or drug delivery agents with proteins. Although, the [Ru(II)(*p*-cymene)(en)Cl]PF_6 and [(η^6-biphenyl)Ru(II)(en)Cl]PF_6 compounds [3], as well as (η^5-Cp*)Rh(III) complexes of some (N,N) polypyridyl ligands showed promising in vitro antiproliferative activity [16], the (η^5-Cp*)Rh(III) complexes of en and bpy possessed negligible effect. Nevertheless, we selected these simple ligands, as they have high and already studied binding affinity to (η^5-Cp*)Rh(III) [53]. Their pM* values calculated under the conditions given in Table 1 are pM* = 12.65 (en) and 13.90 (bpy).

The ternary systems were studied by ^{1}H NMR spectroscopy, which allowed the estimation of the amount of both bound and unbound peptides, as well as en/bpy ligands. The ^{1}H NMR spectra were recorded 24–36 h after the solution preparation, and were then stable by time. Our data (Fig. S16) indicated that the weakest binder GGA-OH does not interact with the (η^5-Cp*)Rh(III)-bpy/en complexes. However, all histidine containing peptides form ternary species with these bidentate ligands (Table 2). The NOESY spectra (Fig. S17) indicate that in all ternary complexes only the C^2H and C^5H protons of imidazole rings are in spatial proximity to the Cp*-methyl protons, i.e. in the ternary species these peptides coordinate monodentately to Rh(III) through their imidazole N^1-nitrogens. These observations also confirm, that considering only monodentate coordination at neutral pH the imidazole ring has much higher (η^5-Cp*)Rh(III) binding ability than carboxylate or amino groups. Moreover, in the cases of **L⁴**, **L⁵** and **L⁶** even the signals of binary peptide complexes appeared on the NMR spectra (Fig. S16), i.e. these peptides are able to displace these strongly coordinating bidentate ligands (en or bpy) from the coordination sphere of (η^5-Cp*)Rh(III). Although the data in Table 2 broadly reflect the thermodynamic stability of binary complexes, the strongest (Cp*)Rh(III)-binder **L⁶** is an exception, since less binary peptide complexes were detected in the ternary systems than expected based on the corresponding pM* values. Due to the unknown values of N-terminal amino p*K*s of imidazole coordinated peptides, the correct evaluation of data in Table 2 is not possible. Nevertheless, an estimation of log $K = 4.5 \pm 0.5$ can be given for the monodentate imidazole coordination to the corresponding en/bpy complexes, i.e. [(η^5-Cp*)Rh(*ab*)Cl] + H_xL = [(η^5-Cp*)Rh(ab)(H_xL)] + Cl^- (where (ab) = en or bpy, L = **L³**, **L⁴**, **L⁵** or **L⁶**, with either neutral (x = 0), or protonated (x = 1) amino group). This values is considerably higher than log $K_3 \sim 3$ obtained in the (η^5-Cp*)Rh(III)-**L^(1(m))** systems (Table 1), indicating some additional interaction(s), which seems to be necessary for efficient binding of [(η^5-Cp*)Rh(ab)] cation to imidazole sidechains of proteins under submilimolar conditions.

Table 2
Percentage of binary and ternary complexes in the (η^5-Cp*)Rh(III)-L2–6-en/bpy 1:1:1 ternary systems at pH 7.4.

Ternary system	binary complex of en/bpy (%)	ternary complex (%)	binary complex of peptide (%)
M-**L²**-en	100	–	–
M-**L³**-en	29	71	–
M-**L⁴**-en	14	12	74
M-**L⁵**-en	–	15	85
M-**L⁶**-en	28	34	38
M-**L²**-bpy	100	–	–
M-**L³**-bpy	25	75	–
M-**L⁴**-bpy	30	62	8
M-**L⁵**-bpy	27	62	11
M-**L⁶**-bpy	28	72	–

2.7. Geometry optimization and stereoisomerism

Although, the (η^5-Cp*)Rh(III) cation is known to form "chiral-at-metal" complexes, the presence of two diastereomers on the NMR spectra was detected only in the (η^5-Cp*)Rh(III)-**L⁶** system. In the other cases, either only one of the two possible diastereomers is formed, or their epimerisation is fast. In order to study this behaviour and to determine the most probable solution structures of peptide complexes present at near physiological pH ($MH_{-1}L$), we performed a computational study using combined molecular mechanical and density functional methods. Applying the Macromodel program and the OPLS3e force field [54] we generated numerous different conformations for each monomer complexes which satisfied the geometrical constraints for the metal-binding sites and the proton-proton proximities obtained from the NMR study. The geometry for the best ranked conformations obtained in this way were then re-optimized at DFT/B3LYP-D3/6-31G(d,p)/LACVP level without any constraints using the Jaguar program [55] (see the Experimental section for the details). The final structures were selected (on energetic ground) from those ones that satisfied the NMR constraints even after optimization. Selected bond lengths and Cartesian coordinates of the optimized structures are listed in Tables S1 and S2, respectively. The calculated Rh-N/Rh-Cl values are somewhat longer (0–0.06 Å for Rh—N, and 0.07–0.11 Å for Rh—Cl) than expected from the related crystal structures [42,56,57], however similar deviations were found in Ru(II) complexes using the DFT/B3LYP/6-31G(d,p)/LANL2DZ method [58].

Bidentate {NH_2,N^-} coordination of a peptide to (η^5-Cp*)Rh(III) allows fast epimerisation of the Rh(III) centre [34,59]. This agrees well with the nearly equal energies of the two optimized diastereomers for [MH_{-1}**L²**] (Fig. S18). On the other hand, tridentate coordination of L-amino acids with $S_{\alpha C}$ absolute configuration results exclusively R configuration for the metal centre [35,38]. Accordingly, our calculation resulted stable structure only for the $R_{Rh}S_{\alpha C}$ diastereomer (Fig. 4) in the case of histidine-amide ([MH_{-1}**L⁴**]$^+$) and HGG-OH ([MH_{-1}**L⁵**]).

In [MH_{-1}**L³**] the GGH-OH peptide has tridentate coordination, i.e. may give a single diastereomer. Although less likely, the 10-membered macrochelate may nonetheless allow the fast epimerisation. The optimized structure of the two diastereomers (Figs. 4A and S18C) show rather strained macrochelates, which would likely prevent the rapid epimerisation. The $S_{Rh}S_{\alpha C}$ diastereomer has more severely distorted ^{3}H-amide group (the sum of the bond angles around the peptide nitrogen is 353.6° vs. 357.3°). More importantly, in the $S_{Rh}S_{\alpha C}$ diastereomer the metal ion is far from the plane determined by the imidazole ring (Fig. S18C), which is highly unusual for imidazole complexes [60]. Consequently, the single set of NMR peaks for [MH_{-1}**L³**] is probably due to the solely presence of the energetically more stable $R_{Rh}S_{\alpha C}$ diastereomer.

In the case of [MH_{-1}**L⁶**]$^+$ we observed two sets of NMR peaks, i.e. the presence of both diastereomers. The isomer ratio is *c.a.* 8:1, therefore proton-proton proximities could be determined only for the major diastereomer. In this case, none of the optimized geometries could fulfil all NOESY constraints, therefore we neglected the Cp*-CH_3-^{3}H-NH proximity constraint, since the ^{3}H-NH proton is not part of the fused (5,6) chelate rings. The most stable structure obtained in this way was a $R_{Rh}S_{\alpha C}$ diastereomer (Fig. 4D), as in all previous cases. Due to the lack of structural information on the minor isomers, we obtained several possible geometries with nearly equal energies (Fig. S18D). However, all of them have at least 3.6 kcal/mol higher energy than the $R_{Rh}S_{\alpha C}$ diastereomer. Although, this energy difference corresponds to a much higher excess of major $R_{Rh}S_{\alpha C}$ diastereomer, we should emphasize, that our calculation was performed in implicit water environment, which cannot completely mimic the presence of a real solvent.

A single set of NMR peaks was detected for the dimer (MH_{-1}**L³**)$_2$ species, too. Discarding the possibility of fast epimerisation, this observation indicates that either the $R_{Rh}S_{\alpha C}/R_{Rh}S_{\alpha C}$ or $S_{Rh}S_{\alpha C}/S_{Rh}S_{\alpha C}$ diastereomer is present in the solution. For these dimer complexes no

conformational search was carried out due to their much higher conformational freedom as compared to the monomer complexes. Instead, we took two (either $R_{Rh}S_{\alpha C}$ or $S_{Rh}S_{\alpha C}$) optimized monomer geometries and connected them by imidazole coordination to obtain a relatively symmetric dimer structure. These initial geometries were minimized with the same DFT (Density Functional Theory) method as in the case of monomers (Fig. S19, for Cartesian coordinates see Table S2). In this case, too, the complex with R configuration around the metal ions ($R_{Rh}S_{\alpha C}/R_{Rh}S_{\alpha C}$ diastereomer) resulted in lower energy, thus probably this isomer is present in the solution.

3. Conclusions

Our goal was to explore the possible interactions of potential metallodrugs ((η^5-Cp*)Rh(III) complexes) and biomolecules (peptides/proteins), in order to understand the most important thermodynamic factors influencing the biospeciation and biotransformation of (η^5-Cp*)Rh(III) complexes. As the imidazole ring of histidine side-chains is one of the main binding sites for (arene)Ru(II)/Rh(III) cations in proteines, first we performed systematic solution thermodynamic, solution structural and computational study on the binary complexes of (η^5-Cp*)Rh(III) cation with histidine containing peptides and their constituents. The comparative evaluation of our solution chemical (pH-potentiometry, UV–Vis, ^{1}H NMR, ESI-MS) data indicated that all the seven studied ligands form highly stable complexes with (η^5-Cp*)Rh(III) cation, which is able to induce the deprotonation of amide nitrogen well below pH 7. Consequently, around the physiological pH the peptide ligands are coordinated to Rh(III) by a tridentate (for **L^2** bidentate) manner, with the participation of amide nitrogen. These observations indicate, that if thermodynamically stable 5/6-membered chelate ring may form with a suitable anchoring (amino or imidazole) group, amide nitrogen is indeed a potential binding site for (η^5-Cp*)Rh(III) in neutral aqueous solution. The calculated pM* values (Table 1), which directly related to the (η^5-Cp*)Rh(III) binding affinity, reflect the following order of thermodynamic stability at pH 7.4: **L^1** ~ **L^{1m}** << **L^2** << **L^3** << **L^4** < **L^5** < **L^6**. Consequently, the observed binding strength essentially depends on the presence and position of histidine unit within the peptide sequence. The ATCUN-motif related GGH-OH (**L^3**) is the weakest (η^5-Cp*)Rh(III) binder, since its tetradentate nature does not fit to the three available (facial) binding sites of (η^5-Cp*)Rh(III). On the other hand, histidine-amide (**L^4**) and HGG-OH (**L^5**) binds considerably stronger to (η^5-Cp*)Rh(III) due to their tridentate facial {N^3_{im},NH_2,N^-} binding sites. Surprisingly, GHG-NH_2 (**L^6**) was found the strongest (η^5-Cp*)Rh(III) binder, despite its preference for meridional coordination geometry.

Based on density functional theory calculations, we also suggested solution structures for all peptide complexes present at near physiological pH. In the cases of tridentately coordinated histidine peptides, the R configuration around the metal ion resulted in the lowest energies.

Having explored the binary (η^5-Cp*)Rh(III)-peptide complexes, we also studied the (η^5-Cp*)Rh(III)-peptide-B ternary systems (where B = 2,2′-bipyridyl or ethylenediamine) in order to mimic the interaction of the (η^5-Cp*)Rh(III)-based potentially anticancer or drug delivery agents with proteins. At pH 7.4, all histidine containing ligands form ternary species with (η^5-Cp*)Rh(III) complexes of strongly coordinating bidentate (N,N) ligands (ethylene-diamine (en) and bipyridyl (bpy)). In these ternary complexes the peptides are monodentately coordinated to Rh(III) through their imidazole N^1-nitrogens, i.e. at physiological pH the monodentate imidazole coordination (log K = 4.5 ± 0.5) provides considerably higher thermodynamic stability than either carboxylate or amino groups. Moreover, in the cases of **L^4**, **L^5** and **L^6** the signals of binary peptide complexes were also present on the NMR spectra of ternary systems, indicating that histidine peptides are able to displace these powerful bidentate ligands (en or bpy) from the coordination sphere of metal ion. These behaviours may have important implication on the biospeciation/ biotransformation of (η^5-Cp*)Rh(III) and related half-sandwich complexes in human bodies.

4. Experimental section

4.1. Materials

All reagents were of analytical grade and used without further purification. KCl, HCl, KOH, 1-methylimidazole (**L^{1m}**, 99%), GGA-OH (**L^2**, 98%), GGH-OH (**L^3**, 98%), HGG-OH (**L^5**) were purchased from Sigma-Aldrich, histidine-amide (**L^4**, 99%) from Bachem AG, imidazole (**L^1**, 99%) from Alfa Aesar, while GHG-NH_2 (**L^6**) was prepared in our laboratory. The (Cp*)Rh(III) stock solution was prepared from [(Cp*)Rh^{III}(μ-Cl)Cl]$_2$ (Sigma-Aldrich, 97%), and was standardized by acid-base titrations.

4.2. Synthesis of GHG-NH_2 (L^6)

GHG-NH_2 peptide (**L^6**) was synthesized on an Fmoc-Rink Amide AM resin (100–200 mesh, 0.71 mmol/g, 0,704 g = 0.5 mmol), using the standard solid phase synthesis protocol with Fmoc-chemistry (Fmoc = Fluorenylmethyloxycarbonyl protecting group). Coupling was performed with DIC (N,N′-Diisopropyl-carbodiimide)/HOBt (Hydroxybenzotriazole) as activating agents, in DMF (Dimethylformamide) with a threefold excess of reagents. After each coupling, Kaiser (ninhydrin) test was performed to check the coupling efficiency. Deprotection was performed with a piperidine/DMF, 1:4 (*v*/v) mixture. After the last deprotection step, 93% TFA (trifluoroacetic acid), a mixture of 2.5% H_2O, 2.5% TIS (triisopropylsilane), and 2% DTT (dithiothreitol) was used for the cleavage for 3 h at 0 °C. After the removal of TFA, the peptide was precipitated with cold diethyl ether, filtered, washed again with diethyl ether, dissolved in 50% aqueous acetic acid, and lyophilized. The crude peptide (yield: 86.6%) was purified using a Phenomenex Jupiter C18 column with a gradient of H_2O:ACN (acetonitrile) 100:0 v/v to H_2O:ACN 70:30 v/v in a presence of 0.1% TFA at a flow rate of 3 cm^3/min and with a gradient of 0.5% ACN/min. Purity control was done by analytical HPLC (Fig. S20A), by High-Resolution ESI-MS spectrometry on a Q Exactive Plus hybrid quadrupole-orbitrap mass spectrometer (Thermo Scientific, Waltham, MA, USA) in a positive ion mode (*m/z* calcd for $C_{10}H_{16}N_6O_3$ $[M + H]^+$ 269.13566, found 269.13568, Fig. S20B), and by ^{1}H NMR (500 MHz, 10% D_2O/H_2O, pH 1.65, δ (ppm): 3.17 (m, 2H, ^{2}H–$C_\beta H_2$), 3.76 (m, 2H, G-CH_2), 3.84 (d, 2H, G-CH_2), 7.23 (d, 2H, J = 232.5 Hz, C(O)-NH_2), 7.24 (s, 1H, C^5—H), 7.94 (br, 1H, ^{3}G-C(O)-NH), 8.52 (s, 1H, C^2—H), 8.75 (s, 1H, ^{2}H-C(O)-NH), Fig. S20C).

4.3. Potentiometric measurements

The protonation and coordination equilibria were investigated by potentiometric titrations in aqueous solution (I = 0.2 M KCl, and T = 298.0 ± 0.1 K) under Ar using an automatic titration set including a computer controlled Dosimat 665 (Metrohm) autoburette and an Orion 710A precision digital pH-meter. The titrations were performed with carbonate-free KOH solution (0.10 M, I = 0.2 M (KCl)). The Metrohm Micro pH glass electrode (125 mm, type 6.0234.100) was calibrated [61] via the modified Nernst Eq. (1):

$$E = E_0 + K.log[H^+] + J_H.[H^+] + \frac{J_{OH}.K_W}{[H^+]} \quad (1)$$

where J_H and J_{OH} are fitting parameters in acidic and alkaline media for the correction of experimental errors, mainly due to the liquid junction and to the alkaline and acidic errors of the glass electrode; $K_w = 10^{-13.76}$ M^2 is the auto-ionization constant of water. The parameters were calculated by the non-linear least squares method. The hydrolysis constants for $[((Cp^*)Rh^{III})_2(OH)_n]^{4-n}$ complexes, where n = 2 or 3, determined in our laboratory (log $\beta_{2-20} = -11.01(1)$, log $\beta_{2-30} = -18.94(2)$) agree well with the literature data [62]. The complex formation was described by a general equilibrium process as follows:

$$pM + qH + rL \leftrightarrow {}^{\beta_{M_pH_qL_r}}_{M_pH_q}{}_{L_r} \quad (2)$$

$$\beta_{M_pH_qL_r} = \frac{[M_pH_qL_r]}{[M]^p[H]^q[L]^r} \quad (3)$$

where M denotes the metal ion, L the non-protonated ligand molecule, and H stands for protons. The corresponding formation constants ($\beta_{MpHqLr} \equiv \beta_{pqr}$) were calculated using the PSEQUAD computer program [63].

The protonation constants were determined from four independent titrations (50–60 data points per titration), with ligand concentration 1.0–6.0 $\times$ 10^{-3} M. The complex formation constants were evaluated from 4 to 7 independent titrations (60–70 data points per titration). The metal-to-ligand ratios were 6:1, 3:1, 2:1, and 1:1. The metal ion concentrations varied between 1.0 and 1.5 $\times$ 10^{-3} M, depending on the metal-to-ligand ratio. The titrations were performed between pH 1.9 and 11.5. pH equilibrium was assumed to be reached if a change in the measured potential was equal or less than 0.2 mV within 2 min. The average waiting time between two doses of titrant solution was 4–6 min up to pH 6, which increased to 6–30 min between pH 6–8 (in this pH region, the (Cp*)Rh(III)-GGH-OH ($\mathbf{L^3}$) system was the slowest, which needed 20–30 min for pH equilibration). Above pH 8 the equilibration was still relatively fast (6–10 min waiting time) in the (Cp*)Rh(III)-1-methylimidazole ($\mathbf{L^1}$) and (Cp*)Rh(III)-GGA-OH ($\mathbf{L^2}$) systems, but the maximal waiting time (30 min) was not enough to attain the pH-equilibrium in the other systems. In these cases, the measured data were evaluated separately, and used only as indicative information (see values in square brackets in Table 1).

4.4. UV–Vis, NMR and ESI-MS measurements

UV–Vis spectra were measured on Thermo Scientific Evolution 200 spectrophotometer using a cell with 2, 1 and 0.5 cm optical pathlengths. The individual UV–Vis spectra of the complexes were calculated by PSEQUAD computer program [63]. The pH-dependent spectrophotometric titrations were performed at 1:1 metal-to-ligand ratio, with $[(Cp^*)Rh^{III}]^{2+}$ concentration of 0.15–0.30 mM, over the pH range 1.9–11.5 at an ionic strength of 0.20 M (KCl) and at $T = 298.0 \pm 0.1$ K. ^{1}H NMR studies were carried out on a Bruker Ultrashield 500 Plus instrument. The ligands were dissolved in a 10% (*v*/v) D_2O/H_2O mixture to yield a concentration of 1–2 mM, and the desired pH was adjusted by HCl/KOH solution at 298.0 $\pm$ 0.1 K and at $I = 0.20$ M KCl, in the absence or presence of $[(Cp^*)Rh^{III}Cl_3]$ at 1:1, 2:3 or 1:4 metal-to-ligand ratios. The chemical shifts (δ) were measured relative to methanol as internal reference and converted to $SiMe_4$ reference using $\delta_{methanol} = 3.35$. Data were processed using the Topspin 2.0 software package (Bruker). High resolution MS spectra were recorded using aqueous solutions without background electrolyte on a Q Exactive Plus hybrid quadrupole-orbitrap mass spectrometer (Thermo Scientific, Waltham, MA, USA) equipped with a heated electrospray ionization (HESI-II) probe that was used in the positive mode, which was coupled to an Abi 140C Syringe Pump.

4.5. Density functional theory calculations

Initial conformations were generated for each of the investigated systems using OPLS3e force-field [55] and a torsional/low-mode sampling method as it is implemented in the Macromodel program of the Schrödinger package [64]. 1000 conformations were generated using the distance constraints derived from the NOESY data. The five highest ranked arrangements were selected for density functional theory geometry optimization. This unconstrained minimization was carried out in two subsequent steps. First the total energy was minimized in vacuum using the B3LYP-D3 [65–67] functional and the 6-31G basis set [68]. For the Rh(III) ion LACVP basis set [69] with effective core potential was applied that also includes relativistic corrections. The geometry obtained this way was further optimized with the help of the same functional, but the basis set was enhanced adding polarization functions to it (6-31G(d,p) [70]). The solvent effects were taken into account employing the polarized continuum model, PCM. The conformations with the lowest total energy fulfilling the NOESY constraints were selected as final structure for each investigated system. For DFT calculations we used the Jaguar program from the Schrödinger package [55] .

Declaration of Competing Interest

The authors declare that they have no known competing financial interests or personal relationships that could have appeared to influence the work reported in this paper.

Acknowledgements

This research was supported by National Research, Development and Innovation Office (NKFIH, Hungary) through the project GINOP-2.3.2-15-2016-00038. A. A. H. thanks Stipendium Hungaricum for her PhD fellowship, which is also supported by the Cultural Affairs & Mission Sector in Egypt. We also acknowledge KIFÜ for awarding us access to computational resources based in Hungary at Debrecen.

Appendix A. Supplementary data

Supplementary data to this article can be found online at https://doi.org/10.1016/j.jinorgbio.2020.111330.

References

[1] G. Gasser, N. Metzler-Nolte, The potential of organometallic complexes in medicinal chemistry, Curr. Opin. Chem. Biol. 16 (2012) 84–91, https://doi.org/10.1016/j.cbpa.2012.01.013.
[2] G. Gasser, I. Ott, N. Metzler-Nolte, Organometallic anticancer compounds, J. Med. Chem. 54 (2011) 3–25, https://doi.org/10.1021/jm100020w.
[3] P. Zhang, P.J. Sadler, Advances in the design of organometallic anticancer complexes, J. Organomet. Chem. 839 (2017) 5–14, https://doi.org/10.1016/j.jorganchem.2017.03.038.
[4] C. Scolaro, A. Bergamo, L. Brescacin, R. Delfino, M. Cocchietto, G. Laurenczy, T. J. Geldbach, G. Sava, P.J. Dyson, In vitro and in vivo evaluation of ruthenium(II)–Arene PTA complexes, J. Med. Chem. 48 (2005) 4161–4171, https://doi.org/10.1021/jm050015d.
[5] W.H. Ang, A. Casini, G. Sava, P.J. Dyson, Organometallic ruthenium-based antitumor compounds with novel modes of action, J. Organomet. Chem. 696 (2011) 989–998, https://doi.org/10.1016/j.jorganchem.2010.11.009.
[6] S. Thota, D.A. Rodrigues, D.C. Crans, E.J. Barreiro, Ru(II) compounds: next-generation anticancer Metallotherapeutics? J. Med. Chem. 61 (2018) 5805–5821, https://doi.org/10.1021/acs.jmedchem.7b01689.
[7] R.G. Kenny, C.J. Marmion, Toward multi-targeted platinum and ruthenium drugs—a new paradigm in cancer drug treatment regimens? Chem. Rev. 119 (2019) 1058–1137, https://doi.org/10.1021/acs.chemrev.8b00271.
[8] W. Su, Y. Li, B. Peng, J. Xie, P. Li, Q. Xiao, S. Huang, Half-sandwich $(Cp^*)RhCl_2$ core complexes containing sulfur donor thiosemicarbazones: synthesis, cytotoxic activity and human serum albumin binding studies, J. Organomet. Chem. 868 (2018) 24–30, https://doi.org/10.1016/j.jorganchem.2018.04.037.
[9] J. Ruiz, V. Rodríguez, N. Cutillas, K.G. Samper, M. Capdevila, Ò. Palacios, A. Espinosa, Novel C,N-chelate rhodium(III) and iridium(III) antitumor complexes incorporating a lipophilic steroidal conjugate and their interaction with DNA, Dalton Trans. 41 (2012) 12847, https://doi.org/10.1039/c2dt31654d.
[10] A.C. Matsheku, M.Y.-H. Chen, S. Jordaan, S. Prince, G.S. Smith, B.C.E. Makhubela, Acridine-containing Ru^{II}, Os^{II}, Rh^{III} and Ir^{III} Half-sandwich complexes: synthesis, structure and antiproliferative activity, Appl. Organomet. Chem. 31 (2017), e3852, https://doi.org/10.1002/aoc.3852.
[11] O. Dömötör, V.F.S. Pape, N.V. May, G. Szakács, É.A. Enyedy, Comparative solution equilibrium studies of antitumor ruthenium(η^6-p-cymene) and rhodium(η^5-C_5Me_5) complexes of 8-hydroxyquinolines, Dalton Trans. 46 (2017) 4382–4396, https://doi.org/10.1039/C7DT00439G.
[12] J.M. Cross, T.R. Blower, N. Gallagher, J.H. Gill, K.L. Rockley, J.W. Walton, Anticancer Ru^{II} and Rh^{III} piano-stool complexes that are histone deacetylase inhibitors, ChemPlusChem. 81 (2016) 1276–1280, https://doi.org/10.1002/cplu.201600413.
[13] A. Kurzwernhart, S. Mokesch, E. Klapproth, M.S. Adib-Ravazi, M.A. Jakupec, C. G. Hartinger, W. Kandioller, B.K. Keppler, Flavonoid-based organometallics with different metal centers - investigations of the effects on reactivity and cytotoxicity: flavonoid-based organometallics with different metal centers, Eur. J. Inorg. Chem. 2016 (2016) 240–246, https://doi.org/10.1002/ejic.201501020.

[14] G.S. Yellol, A. Donaire, J.G. Yellol, V. Vasylyeva, C. Janiak, J. Ruiz, On the antitumor properties of novel cyclometalated benzimidazole Ru(II), Ir(III) and Rh (III) complexes, Chem. Commun. 49 (2013) 11533, https://doi.org/10.1039/c3cc46239k.

[15] C.K. Rono, W.K. Chu, J. Darkwa, D. Meyer, B.C.E. Makhubela, Triazolyl Ru^{II} , Rh^{III} , Os^{II} , and Ir^{III} complexes as potential anticancer agents: Synthesis, structure elucidation, cytotoxicity, and DNA model interaction studies, Organometallics. 38 (2019) 3197–3211, https://doi.org/10.1021/acs.organomet.9b00440.

[16] M.A. Scharwitz, I. Ott, Y. Geldmacher, R. Gust, W.S. Sheldrick, Cytotoxic half-sandwich rhodium(III) complexes: Polypyridyl ligand influence on their DNA binding properties and cellular uptake, J. Organomet. Chem. 693 (2008) 2299–2309, https://doi.org/10.1016/j.jorganchem.2008.04.002.

[17] S. Thangavel, M. Paulpandi, H.B. Friedrich, K. Murugan, S. Kalva, A.A. Skelton, Synthesis, characterization, antiproliferative and molecular docking study of new half sandwich Ir(III), Rh(III) and Ru(II) complexes, J. Inorg. Biochem. 159 (2016) 50–61, https://doi.org/10.1016/j.jinorgbio.2016.02.006.

[18] J. Markham, J. Liang, A. Levina, R. Mak, B. Johannessen, P. Kappen, C.J. Glover, B. Lai, S. Vogt, P.A. Lay, (Pentamethylcyclopentadienato)rhodium complexes for delivery of the curcumin anticancer drug: (Pentamethylcyclopentadienato) rhodium complexes for delivery of the curcumin anticancer drug, Eur. J. Inorg. Chem. 2017 (2017) 1812–1823, https://doi.org/10.1002/ejic.201601331.

[19] Z. Adhireksan, G.E. Davey, P. Campomanes, M. Groessl, C.M. Clavel, H. Yu, A. A. Nazarov, C.H.F. Yeo, W.H. Ang, P. Dröge, U. Rothlisberger, P.J. Dyson, C. A. Davey, Ligand substitutions between ruthenium–cymene compounds can control protein versus DNA targeting and anticancer activity, Nat. Commun. 5 (2014) 3462, https://doi.org/10.1038/ncomms4462.

[20] F. Wang, J. Bella, J.A. Parkinson, P.J. Sadler, Competitive reactions of a ruthenium arene anticancer complex with histidine, cytochrome c and an oligonucleotide, JBIC J. Biol. Inorg. Chem. 10 (2005) 147–155, https://doi.org/10.1007/s00775-004-0621-5.

[21] J. Will, A. Kyas, W.S. Sheldrick, D. Wolters, Identification of (η6-arene)ruthenium (II) protein binding sites in *E. coli* cells by combined multidimensional liquid chromatography and ESI tandem mass spectrometry: specific binding of [(η6-p-cymene)RuCl2(DMSO)] to stress-regulated proteins and to helicases, JBIC J. Biol. Inorg. Chem. 12 (2007) 883–894, https://doi.org/10.1007/s00775-007-0242-x.

[22] C. Scolaro, A.B. Chaplin, C.G. Hartinger, A. Bergamo, M. Cocchietto, B.K. Keppler, G. Sava, P.J. Dyson, Tuning the hydrophobicity of ruthenium(ii)–arene (RAPTA) drugs to modify uptake, biomolecular interactions and efficacy, Dalton Trans. 5065 (2007), https://doi.org/10.1039/b705449a.

[23] A. Casini, G. Mastrobuoni, W.H. Ang, C. Gabbiani, G. Pieraccini, G. Moneti, P. J. Dyson, L. Messori, ESI–MS characterisation of protein adducts of anticancer ruthenium(II)-Arene PTA (RAPTA) complexes, ChemMedChem. 2 (2007) 631–635, https://doi.org/10.1002/cmdc.200600258.

[24] S.M. Meier, M. Hanif, W. Kandioller, B.K. Keppler, C.G. Hartinger, Biomolecule binding vs. anticancer activity: Reactions of Ru(arene)[(thio)pyr-(id)one] compounds with amino acids and proteins, J. Inorg. Biochem. 108 (2012) 91–95, https://doi.org/10.1016/j.jinorgbio.2011.08.011.

[25] W. Kandioller, E. Balsano, S.M. Meier, U. Jungwirth, S. Göschl, A. Roller, M. A. Jakupec, W. Berger, B.K. Keppler, C.G. Hartinger, Organometallic anticancer complexes of lapachol: metal Centre-dependent formation of reactive oxygen species and correlation with cytotoxicity, Chem. Commun. 49 (2013) 3348, https://doi.org/10.1039/c3cc40432c.

[26] A. Merlino, Interactions between proteins and Ru compounds of medicinal interest: a structural perspective, Coord. Chem. Rev. 326 (2016) 111–134, https://doi.org/10.1016/j.ccr.2016.08.001.

[27] I.W. McNae, K. Fishburne, A. Habtemariam, T.M. Hunter, M. Melchart, F. Wang, M. D. Walkinshaw, P.J. Sadler, Half-sandwich arene ruthenium(II)–enzyme complex, Chem. Commun. (2004) 1786–1787, https://doi.org/10.1039/B408141B.

[28] W.H. Ang, L.J. Parker, A. De Luca, L. Juillerat-Jeanneret, C.J. Morton, M. Lo Bello, M.W. Parker, P.J. Dyson, Rational Design of an Organometallic Glutathione Transferase Inhibitor, Angew. Chem. Int. Ed. 48 (2009) 3854–3857, https://doi.org/10.1002/anie.200900185.

[29] B. Wu, M.S. Ong, M. Groessl, Z. Adhireksan, C.G. Hartinger, P.J. Dyson, C. A. Davey, A ruthenium Antimetastasis agent forms specific histone protein adducts in the nucleosome Core, Chem. Eur. J. 17 (2011) 3562–3566, https://doi.org/10.1002/chem.201100298.

[30] Y. Takezawa, P. Böckmann, N. Sugi, Z. Wang, S. Abe, T. Murakami, T. Hikage, G. Erker, Y. Watanabe, S. Kitagawa, T. Ueno, Incorporation of organometallic Ru complexes into apo-ferritin cage, Dalton Trans. 40 (2011) 2190–2195, https://doi.org/10.1039/C0DT00955E.

[31] S.M. Meier, M. Hanif, Z. Adhireksan, V. Pichler, M. Novak, E. Jirkovsky, M. A. Jakupec, V.B. Arion, C.A. Davey, B.K. Keppler, C.G. Hartinger, Novel metal(II) arene 2-pyridinecarbothioamides: a rationale to orally active organometallic anticancer agents, Chem. Sci. 4 (2013) 1837, https://doi.org/10.1039/c3sc22294b.

[32] J.M. Zimbron, T. Heinisch, M. Schmid, D. Hamels, E.S. Nogueira, T. Schirmer, T. R. Ward, A dual anchoring strategy for the localization and activation of artificial Metalloenzymes based on the biotin–streptavidin technology, J. Am. Chem. Soc. 135 (2013) 5384–5388, https://doi.org/10.1021/ja309974s.

[33] O. Dömötör, É.A. Enyedy, Binding mechanisms of half-sandwich Rh(III) and Ru(II) arene complexes on human serum albumin: a comparative study, J. Biol. Inorg. Chem. JBIC Publ. Soc. Biol. Inorg. Chem. 24 (2019) 703–719, https://doi.org/10.1007/s00775-019-01683-0.

[34] K. Severin, R. Bergs, W. Beck, Bioorganometallic chemistry - transition metal complexes with α-amino acids and peptides, Angew. Chem. Int. Ed. Eng. 37 (1998) 1634–1654, https://doi.org/10.1002/(SICI)1521-3773(19980703)37:12<1634::AID-ANIE1634>3.0.CO;2-C.

[35] F.A. Egbewande, L.E.H. Paul, B. Therrien, J. Furrer, Synthesis, characterization and cytotoxicity of (η^6-p-cymene)ruthenium(II) complexes of α-amino acids, Eur. J. Inorg. Chem. 2014 (2014) 1174–1184, https://doi.org/10.1002/ejic.201301297.

[36] L. Bíró, E. Balogh, P. Buglyó, Interaction between $[Ru(\eta^6\text{-p-cym})(H_2O)_3]^{2+}$ and DL-serine or DL-isoserine: The role of the side chain alcoholic OH group in metal ion binding, J. Organomet. Chem. 734 (2013) 61–68, https://doi.org/10.1016/j.jorganchem.2012.11.023.

[37] J. Patalenszki, L. Bíró, A.C. Bényei, T.R. Muchova, J. Kasparkova, P. Buglyó, Half-sandwich complexes of ruthenium, osmium, rhodium and iridium with DL -methionine or S-methyl- L -cysteine: a solid state and solution equilibrium study, RSC Adv. 5 (2015) 8094–8107, https://doi.org/10.1039/C4RA15649H.

[38] W.S. Sheldrick, S. Heeb, Synthesis and structural characterization of η6-arene-ruthenium(II) complexes of α-amino acids with coordinating side chains, J. Organomet. Chem. 377 (1989) 357–366, https://doi.org/10.1016/0022-328X(89)80097-X.

[39] B.S. Murray, L. Menin, R. Scopelliti, P.J. Dyson, Conformational control of anticancer activity: the application of arene-linked dinuclear ruthenium(II) organometallics, Chem. Sci. 5 (2014) 2536–2545, https://doi.org/10.1039/C4SC00116H.

[40] R.H. Wills, A. Habtemariam, A.F. Lopez-Clavijo, M.P. Barrow, P.J. Sadler, P. B. O'Connor, Insights into the binding sites of organometallic ruthenium anticancer compounds on peptides using ultra-high resolution mass spectrometry, J. Am. Soc. Mass Spectrom. 25 (2014) 662–672, https://doi.org/10.1021/jasms.8b04745.

[41] F. Wang, J. Xu, A. Habtemariam, J. Bella, P.J. Sadler, Competition between glutathione and guanine for a ruthenium(II) Arene anticancer complex: detection of a Sulfenato intermediate, J. Am. Chem. Soc. 127 (2005) 17734–17743, https://doi.org/10.1021/ja053387k.

[42] C. Robl, M. Maurus, K. Sünkel, W. Beck, R. Krämer, K. Polborn, Organometallic half-Sandwich complexes promote the formation of linear Oligopeptides from amino acid esters, Chem. Eur. J. 2 (1996) 1518–1526, https://doi.org/10.1002/chem.19960021208.

[43] B.D. Balogh, Z. Bihari, P. Buglyó, G. Csire, Z. Kerekes, M. Lukács, I. Sóvágó, K. Várnagy, Metal binding selectivity of an N-terminally free multihistidine peptide HAVAHHH-NH2, New J. Chem. 43 (2019) 907–916, https://doi.org/10.1039/C8NJ04538K.

[44] Z. Bihari, V. Ugone, E. Garribba, N. Lihi, P. Buglyó, Complex formation between $[(\eta^6\text{-p-cym})Ru(H_2O)_3]^{2+}$ and oligopeptides containing three histidyl moieties, J. Organomet. Chem. 823 (2016) 116–125, https://doi.org/10.1016/j.jorganchem.2016.09.013.

[45] H.B. Albada, F. Wieberneit, I. Dijkgraaf, J.H. Harvey, J.L. Whistler, R. Stoll, N. Metzler-Nolte, R.H. Fish, The Chemoselective reactions of tyrosine-containing G-protein-coupled receptor peptides with $[Cp^*Rh(H_2O)_3](OTf)_2$, including 2D NMR structures and the biological consequences, J. Am. Chem. Soc. 134 (2012) 10321–10324, https://doi.org/10.1021/ja303010k.

[46] A. Buryak, K. Severin, An organometallic chemosensor for the sequence-selective detection of Histidine- and methionine-containing peptides in water at neutral pH, Angew. Chem. Int. Ed. 43 (2004) 4771–4774, https://doi.org/10.1002/anie.200460808.

[47] A. Ozsváth, L. Bíró, E.M. Nagy, P. Buglyó, D. Sanna, E. Farkas, Trends and exceptions in the interaction of hydroxamic acid derivatives of common Di- and tripeptides with some 3d and 4d metal ions in aqueous solution, Molecules. 24 (2019) 3941, https://doi.org/10.3390/molecules24213941.

[48] SCQuery, The IUPAC Stability Constants Database, Academic Software, R. Soc. Chem, 2005.

[49] Z. Bihari, Z. Nagy, P. Buglyó, $[(\eta^6\text{-p-cym})Ru(H_2O)_3]^{2+}$ binding capability of N-methylimidazole to model the interaction between the metal ion and surface histidine residues of peptides, J. Organomet. Chem. 782 (2015) 82–88, https://doi.org/10.1016/j.jorganchem.2014.12.026.

[50] M.-L. Lehaire, R. Scopelliti, L. Herdeis, K. Polborn, P. Mayer, K. Severin, Diastereoselective formation of Metallamacrocyclic (Arene)Ru^{II} and Cp^*Rh^{III} complexes, Inorg. Chem. 43 (2004) 1609–1617, https://doi.org/10.1021/ic035328i.

[51] H. Kozłowski, W. Bal, M. Dyba, T. Kowalik-Jankowska, Specific structure–stability relations in metallopeptides, Coord. Chem. Rev. 184 (1999) 319–346, https://doi.org/10.1016/S0010-8545(98)00261-6.

[52] I. Sóvágó, K. Várnagy, N. Lihi, Á. Grenács, Coordinating properties of peptides containing histidyl residues, Coord. Chem. Rev. 327–328 (2016) 43–54, https://doi.org/10.1016/j.ccr.2016.04.015.

[53] É.A. Enyedy, J.P. Mészáros, O. Dömötör, C.M. Hackl, A. Roller, B.K. Keppler, W. Kandioller, Comparative solution equilibrium studies on pentamethylcyclopentadienyl rhodium complexes of 2,2′-bipyridine and ethylenediamine and their interaction with human serum albumin, J. Inorg. Biochem. 152 (2015) 93–103, https://doi.org/10.1016/j.jinorgbio.2015.08.025.

[54] E. Harder, W. Damm, J. Maple, C. Wu, M. Reboul, J.Y. Xiang, L. Wang, D. Lupyan, M.K. Dahlgren, J.L. Knight, J.W. Kaus, D.S. Cerutti, G. Krilov, W.L. Jorgensen, R. Abel, R.A. Friesner, OPLS3: a force field providing broad coverage of drug-like small molecules and proteins, J. Chem. Theory Comput. 12 (2016) 281–296, https://doi.org/10.1021/acs.jctc.5b00864.

[55] A.D. Bochevarov, E. Harder, T.F. Hughes, J.R. Greenwood, D.A. Braden, D. M. Philipp, D. Rinaldo, M.D. Halls, J. Zhang, R.A. Friesner, Jaguar: a high-performance quantum chemistry software program with strengths in life and materials sciences, Int. J. Quantum Chem. 113 (2013) 2110–2142, https://doi.org/10.1002/qua.24481.

[56] A. Becerra, R. Contreras, D. Carmona, F.J. Lahoz, P. García-Orduña, Half-sandwich rhodium and iridium complexes containing homochiral imidazolyl-imine ligands: synthesis, characterization and catalytic applications, Dalton Trans. 42 (2013) 11640, https://doi.org/10.1039/c3dt51222c.
[57] A. Gilewska, B. Barszcz, J. Masternak, K. Kazimierczuk, J. Sitkowski, J. Wietrzyk, E. Turlej, Similarities and differences in d^6 low-spin ruthenium, rhodium and iridium half-sandwich complexes: synthesis, structure, cytotoxicity and interaction with biological targets, J. Biol. Inorg. Chem. JBIC Publ. Soc. Biol. Inorg. Chem. 24 (2019) 591–606, https://doi.org/10.1007/s00775-019-01665-2.
[58] T.G. Scrase, M.J. O'Neill, A.J. Peel, P.W. Senior, P.D. Matthews, H. Shi, S.R. Boss, P.D. Barker, Selective lability of ruthenium(II) arene amino acid complexes, Inorg. Chem. 54 (2015) 3118–3124, https://doi.org/10.1021/ic502051y.
[59] W. Beck, R. Krämer, Directed synthesis of peptides from α-amino acid esters at metal centers, Angew. Chem. Int. Ed. Eng. 30 (1991) 1467–1469, https://doi.org/10.1002/anie.199114671.
[60] P. Chakrabarti, Geometry of interaction of metal ions with histidine residues in protein structures, Protein Eng. Des. Sel. 4 (1990) 57–63, https://doi.org/10.1093/protein/4.1.57.
[61] F.J.C. Rossotti, H. Rossotti, The Determination of Stability Constants and Other Equilibrium Constants in Solution, McGraw-Hill Book Co., New York, 1962.
[62] O. Dömötör, S. Aicher, M. Schmidlehner, M.S. Novak, A. Roller, M.A. Jakupec, W. Kandioller, C.G. Hartinger, B.K. Keppler, É.A. Enyedy, Antitumor pentamethylcyclopentadienyl rhodium complexes of maltol and allomaltol: synthesis, solution speciation and bioactivity, J. Inorg. Biochem. 134 (2014) 57–65, https://doi.org/10.1016/j.jinorgbio.2014.01.020.
[63] L. Zékány, I. Nagypál, G. Peintler, PSEQUAD for chemical equilibria, Technical Software Distributors, Baltimore, MD, 1991.
[64] Schrödinger Release 2019–4:. MacroModel, Schrödinger, LLC, New York, NY, 2019.
[65] P.J. Stephens, F.J. Devlin, C.F. Chabalowski, M.J. Frisch, Ab initio calculation of vibrational absorption and circular Dichroism spectra using density functional force fields, J. Phys. Chem. 98 (1994) 11623–11627, https://doi.org/10.1021/j100096a001.
[66] S. Grimme, J. Antony, S. Ehrlich, H. Krieg, A consistent and accurate ab initio parametrization of density functional dispersion correction (DFT-D) for the 94 elements H-Pu, J. Chem. Phys. 132 (2010) 154104, https://doi.org/10.1063/1.3382344.
[67] L. Goerigk, S. Grimme, A thorough benchmark of density functional methods for general main group thermochemistry, kinetics, and noncovalent interactions, Phys. Chem. Chem. Phys. 13 (2011) 6670, https://doi.org/10.1039/c0cp02984j.
[68] W.J. Hehre, R. Ditchfield, J.A. Pople, Self—consistent molecular orbital methods. XII. Further extensions of Gaussian—type basis sets for use in molecular orbital studies of organic molecules, J. Chem. Phys. 56 (1972) 2257–2261, https://doi.org/10.1063/1.1677527.
[69] P.J. Hay, W.R. Wadt, Ab initio effective core potentials for molecular calculations. Potentials for the transition metal atoms Sc to Hg, J. Chem. Phys. 82 (1985) 270–283, https://doi.org/10.1063/1.448799.
[70] M.M. Francl, W.J. Pietro, W.J. Hehre, J.S. Binkley, M.S. Gordon, D.J. DeFrees, J. A. Pople, Self-consistent molecular orbital methods. XXIII. A polarization-type basis set for second-row elements, J. Chem. Phys. 77 (1982) 3654–3665, https://doi.org/10.1063/1.444267.